J|A|C|S
ARTICLES
Published on Web 10/11/2002

Anisotropic NMR Interaction Tensors in the Decamethylaluminocenium Cation

Robert W. Schurko,*,† Ivan Hung,† Charles L. B. Macdonald,‡ and Alan H. Cowley‡

Contribution from the Department of Chemistry and Biochemistry, University of Windsor, Windsor, Ontario, Canada N9B 3P4, and Department of Chemistry, University of Texas at Austin, Austin, Texas 78712

Received March 18, 2002

Abstract: Solid-state NMR experiments, analytical and numerical simulations of solid NMR powder patterns, ab initio self-consistent field and hybrid density functional theory calculations, and single-crystal X-ray diffraction are used to characterize the molecular structure and anisotropic NMR interaction tensors in the bis(pentamethylcyclopentadienyl)aluminum cation, $[Cp^*_2Al]^+$. This highly symmetric main group metallocene has a structure analogous to that of ferrocene and the cobaltocenium cation. The single-crystal X-ray diffraction structure is reported for $[Cp^*_2Al][AlCl_4]$. Solid-state $^{27}Al\{^1H\}$ magic-angle spinning and static NMR experiments are used to study the aluminum chemical shielding and electric field gradient tensors, revealing axial symmetry in both cases with a large chemical shielding span of $\Omega = 83(3)$ ppm and a small nuclear quadrupole coupling constant, $C_Q(^{27}Al) = 0.86(10)$ MHz. Carbon-13 CPMAS NMR experiments in combination with ab initio calculations and simulations of the effects of chemical exchange on ^{13}C static powder patterns reveal dynamic rotation of rings and suggest a low internal rotational barrier for this process. Theoretical computations of interaction tensors using the Gaussian 98 and Amsterdam Density Functional software packages are in good agreement with experiment and lend insight into the molecular origin of these NMR interactions. Orientations of the NMR tensors determined from theory, the large chemical shielding span, and the very small value of $C_Q(^{27}Al)$ can all be rationalized in terms of the high molecular symmetry.

Introduction

There recently has been renewed interest in the important class of organometallic complexes analogous to ferrocene, known as the metallocenes.[1−3] Metallocenes have the general formula Cp'_2M, where Cp′ is a cyclopentadienyl ring ($C_5R_5^-$, R = H, Me, Ph, Bz, etc., Cp* = C_5Me_5). Much of the current research on metallocenes focuses upon main group and early transition metal metallocenes. The former are fascinating from the standpoint of their unique structural properties and the rich variety of metal-p-π-bonding interactions, while the latter find application in a variety of catalytic, polymerization, and metal chemical vapor deposition processes.[4,5]

Metallocenes represent ideal complexes for study by solid-state NMR methods, as examination of orientation-dependent NMR interactions provides detailed information on molecular structure and intramolecular motion in these complexes. For instance, solid-state ^{13}C NMR studies have been conducted on a variety of metallocenes to study ring motion, ^{13}C chemical shielding tensors, and *J*-coupling.[6−10] Solid-state deuterium NMR has also been used to examine motion of oriented cobaltocene molecules in several instances.[11] Surprisingly, despite the numerous solution NMR studies on metallocenes and related organometallic complexes,[12] relatively few solid-state NMR experiments have been reported on the central metal nucleus. This list includes a ^7Li NMR study of lithocenes,[13] ^{23}Na NMR of CpNa-TMEDA,[14] ^{119}Sn and ^{207}Pb NMR characterizations of a variety of stannocenes and plumbocenes,[15,16] a

* To whom correspondence should be addressed. E-mail: rschurko@uwindsor.ca.
† University of Windsor.
‡ University of Texas at Austin.

(1) *Metallocenes Vol. 1: Synthesis, Reactivity, Applications*; Togni, A., Halterman, R. L., Eds.; Wiley-VCH Verlag GmbH: Weinheim, 1998.
(2) Harder, S. *Coord. Chem. Rev.* **1998**, *176*, 17.
(3) Jutzi, P.; Burford, N. *Chem. Rev.* **1999**, *99*, 969.
(4) *Metallocenes Vol. 2: Synthesis, Reactivity, Applications*; Togni, A., Halterman, R. L., Eds.; Wiley-VCH Verlag GmbH: Weinheim, 1998.
(5) Beswick, M. A.; Palmer, J. S.; Wright, D. S. *Chem. Soc. Rev.* **1998**, *27*, 225.
(6) (a) Heise, H.; Köhler, F. H.; Xie, X. L. *J. Magn. Reson.* **2001**, *150*, 198. (b) Heise, H.; Köhler, F. H.; Brouwer, E. B.; Harris, R. K.; Steuernagel, S. *Magn. Reson. Chem.* **1999**, *37*, 573. (c) Köhler, F. H.; Xie, X. L. *Magn. Reson. Chem.* **1997**, *35*, 487. (d) Blümel, J.; Herker, M.; Hiller, W.; Köhler, F. H. *Organometallics* **1996**, *15*, 3474.
(7) Orendt, A. M.; Facelli, J. C.; Jiang, Y. J.; Grant, D. M. *J. Phys. Chem. A* **1998**, *102*, 7692.
(8) (a) Wemmer, D. E.; Ruben, D. J.; Pines, A. *J. Am. Chem. Soc.* **1981**, *103*, 28. (b) Wemmer, D. E.; Pines, A. *J. Am. Chem. Soc.* **1981**, *103*, 34.
(9) (a) Heyes, S. J.; Dobson, C. M. *J. Am. Chem. Soc.* **1991**, *113*, 463. (b) Munson, E. J.; Douskey, M. C.; De Paul, S. M.; Ziegeweid, M.; Phillips, L.; Separovic, F.; Davies, M. S.; Aroney, M. J. *J. Organomet. Chem.* **1999**, *577*, 19.
(10) (a) Campbell, A. J.; Fyfe, C. A.; Goel, R. G.; Maslowsky, E.; Senoff, C. V. *J. Am. Chem. Soc.* **1972**, *94*, 8387. (b) Kentgens, A. P. M.; Karrenbald, H.; de Boer, E.; Schumann, H. *J. Organomet. Chem.* **1992**, *429*, 99.
(11) (a) Evans, J. S. O.; O'Hare, D.; Clement, R. *J. Am. Chem. Soc.* **1995**, *117*, 4595. (b) Mason, S. J.; Heyes, S. J.; O'Hare, D. *J. Chem. Soc., Chem. Commun.* **1995**, 1657.
(12) (a) von Philipsborn, W. *Chem. Soc. Rev.* **1999**, *28*, 95. (b) Rehder, D. *Coord. Chem. Rev.* **1991**, *110*, 161. (c) Benn, R.; Rufińska, A. *Angew. Chem., Int. Ed. Engl.* **1986**, *25*, 861.
(13) Johnels, D.; Boman, A.; Edlund, U. *Magn. Reson. Chem.* **1998**, *36*, S151.
(14) Pietrass, T.; Burkert, P. K. *Inorg. Chim. Acta* **1993**, *207*, 253.

10.1021/ja020394p CCC: $22.00

single-crystal ^{59}Co NMR study of $[Cp_2Co]NO_3 \cdot H_2O$,[17] and a ^{171}Yb CPMAS NMR study of $Cp'_2Yb(II)$ complexes.[18] In this paper, we report an experimental solid-state NMR and single-crystal X-ray study for the decamethylaluminocenium salt, $[Cp^*_2Al][AlCl_4]$. The decamethylaluminocenium cation has a highly symmetric, ferrocene-like D_{5d} structure with a staggered conformation of the Cp* rings (ignoring the methyl protons).

Aluminum-27 is a quadrupolar nucleus (nuclear spin $S = {}^5/_2$) with a moderately sized nuclear quadrupole moment ($Q(^{27}Al) = 1.403 \times 10^{-29}$ m^2)[19] and is well suited for solid-state NMR experiments due to its 100% natural abundance and magnetogyric ratio comparable to ^{13}C.[20] The ^{27}Al NMR spectrum typically consists of a central transition affected by the second-order quadrupolar interaction. The quadrupolar interaction is the interaction between the nuclear quadrupole moment and the electric field gradient (EFG) at the nucleus, which is defined by a traceless 3×3 tensor with principal components $|V_{11}| \leq |V_{22}| \leq |V_{33}|$. The magnitude and asymmetry of this interaction are given by the nuclear quadrupole coupling constant, $C_Q = e^2Qq/h = eQV_{33}/h$, and asymmetry parameter, $\eta_Q = (V_{11} - V_{22})/V_{33}$.

Many isotropic ^{27}Al chemical shifts have been reported in the literature, indicating a chemical shift range of about 300 ppm.[21,22] It has recently been demonstrated that solid-state ^{27}Al NMR spectra may also be influenced by anisotropic chemical shielding interactions (vide infra). The chemical shielding (CS) tensor is a 3×3 tensor, with three principal components defined with respect to the unshielded bare nucleus (i.e., $\sigma = 0$) from low to high magnetic shielding as $\sigma_{11} \leq \sigma_{22} \leq \sigma_{33}$. The isotropic chemical shielding is the average of the trace, $\sigma_{iso} = (\sigma_{11} + \sigma_{22} + \sigma_{33})/3$, and the breadth and asymmetry of the chemical shielding tensor are described by the span, $\Omega = \sigma_{33} - \sigma_{11}$, and the skew, $\kappa = 3(\sigma_{iso} - \sigma_{22})/\Omega$, respectively. These expressions can also be recast in terms of chemical shift, which is approximately related to chemical shielding by[23]

$$\delta_{sample} = \frac{\sigma_{ref} - \sigma_{sample}}{1 - \sigma_{ref}} \times 10^6 \approx \sigma_{ref} - \sigma_{sample} \qquad (1)$$

where σ_{ref} is the absolute chemical shielding for some reference compound. Thus, the chemical shift tensor, from least to most shielded, has principal components $\delta_{11} \geq \delta_{22} \geq \delta_{33}$, with $\delta_{iso} = (\delta_{11} + \delta_{22} + \delta_{33})/3$, $\Omega = \delta_{11} - \delta_{33}$, and $\kappa = 3(\delta_{22} - \delta_{iso})/\Omega$.

Very few instances of aluminum chemical shielding anisotropy (CSA) have been reported, including ^{27}Al NMR studies on single crystals of α-Al_2O_3,[24] powder samples of four-coordinate $AlCl_3OPCl_3$,[25] and hexacoordinate tridentate aluminum complexes.[26] From a theoretical standpoint, ab initio restricted Hartree−Fock (RHF) and hybrid density functional theory (DFT) studies of diatomic aluminum complexes indicate that aluminum CSA will be significant in molecules in which the aluminum is in a linear environment.[26] Given the foregoing lack of information, there is a clear need for additional experimental studies of anisotropic magnetic shielding tensors for aluminum (as well as other group 13 elements).

In the present paper, we report the results of solid-state ^{27}Al magic-angle spinning (MAS) and static (i.e., stationary sample) NMR experiments on $[Cp^*_2Al][AlCl_4]$, which reveal (i) a small quadrupolar interaction at the metallocene aluminum nucleus, (ii) two crystallographically distinct metallocene sites in the unit cell, and (iii) an axially symmetric aluminum shielding tensor with a large span. CS and EFG tensors for metal nuclei Cp'_nM-type compounds have been previously reported only for Cp_2Sn,[15] $[(\eta^5\text{-}Cp)_2Sn(\mu\text{-}Cp)NaPMDETA]$,[16] and CpLi.[13] Carbon-13 CPMAS NMR spectra are also presented, along with chemical shielding tensors of the aromatic Cp* carbons. Our experimental efforts are accompanied by a detailed series of RHF and hybrid DFT calculations of EFG and CS tensors. Pure DFT calculations are used to provide an analysis of which molecular orbitals make major contributions to magnetic shielding of the aluminum nucleus. A simple chemical exchange model is presented which explains the discrepancies between experimental and theoretical carbon chemical shielding tensors. Our overall objective is to provide insights into the relationships between molecular symmetry and dynamics, electronic structure, and NMR interaction tensors in this important class of compounds.

Experimental Section

General Methods. Pentamethylcyclopentadiene (Cp*H) was synthesized according to a published procedure.[27] Aluminum(III) chloride and all other reagents were obtained from the Aldrich Chemical Co. and were used as received. Diethyl ether, hexanes, and toluene were dried over sodium with benzophenone, and CH_2Cl_2 was dried over CaH_2. All solvents were distilled and degassed immediately prior to use. All reagents were handled in argon-filled gloveboxes (Vacuum Atmospheres or MBraun), and reactions were performed using standard inert-atmosphere techniques. Melting points were recorded in sealed capillaries on an Electrothermal apparatus and are uncorrected. Solution NMR spectra were recorded on a General Electric QE-300 NMR spectrometer with frequencies of 300.19 MHz for ^{1}H, 75.48 MHz for ^{13}C, and 78.31 MHz for ^{27}Al. Solution NMR samples were either run immediately after removal from the glovebox or flame-sealed in 5 mm NMR tubes. All solution chemical shifts are reported in ppm relative to an external standard (TMS for ^{1}H and ^{13}C, $[Al(D_2O)_6]^{3+}$ for ^{27}Al). Low-resolution mass spectra (CI, CH_4) were obtained on a Finnigan MAT TSQ 700 instrument. High-resolution mass spectra (CI, CH_4) were obtained on a VG ZAB-VE sector instrument. Cp^*_2AlCl was prepared by a slight variation of the reported method.[28]

Preparation of $[Cp^*_2Al][AlCl_4]$. A suspension of Al_2Cl_6 (0.40 g, 1.50 mmol) in CH_2Cl_2 (40 mL) was added to a stirred pale yellow

(15) (a) Janiak, C.; Schumann, H.; Stader, C.; Wrackmeyer, B.; Zuckerman, J. J. *Chem. Ber.* **1988**, *121*, 1745. (b) Wrackmeyer, B.; Kupçe, E. Kehr, G.; Sebald, A. *Magn. Reson. Chem.* **1992**, *30*, 964.
(16) Armstrong, D. R.; Duer, M. J.; Davidson, M. G.; Moncrieff, D.; Russell, C. A.; Stourton, C.; Steiner, A.; Stalke, D.; Wright, D. S. *Organometallics* **1997**, *16*, 3340.
(17) Spiess, H. W.; Haas, H.; Hartmann, H. *J. Chem. Phys.* **1969**, *50*, 3057.
(18) Keates, J. M.; Lawless, G. A. *Organometallics* **1997**, *16*, 2842.
(19) (a) Sundholm, D.; Olsen, J. *Phys. Rev. A* **1993**, *47*, 2672. (b) Pyykkö, P. *Z. Naturforsch.* **1992**, *47a*, 189.
(20) Smith, M. E. *Appl. Magn. Reson.* **1993**, *4*, 1.
(21) Delpuech, J. J. In *NMR of Newly Accessible Nuclei − Volume 2: Chemically and Biochemically Important Elements*; Laszlo, P., Ed.; Academic Press: New York, 1983; pp 153−195.
(22) Akitt, J. W. *Prog. Nucl. Magn. Reson. Spectrosc.* **1989**, *21*, 1.
(23) (a) Jameson, C. J.; Mason, J. In *Multinuclear NMR*; Mason, J., Ed.; Plenum Press: New York, 1987; pp 51−83. (b) Jameson, C. J. In *Encyclopedia of Nuclear Magnetic Resonance*; Grant, D. M., Harris, R. K., Eds.; John Wiley & Sons: Chichester, U.K., 1996; pp 1273−1281.
(24) Vosegaard, T.; Jakobsen, H. J. *J. Magn. Reson.* **1997**, *128*, 135.
(25) Schurko, R. W.; Wasylishen, R. E.; Phillips, A. D. *J. Magn. Reson.* **1998**, *133*, 388.
(26) Schurko, R. W.; Wasylishen, R. E.; Foerster, H. *J. Phys. Chem. A* **1998**, *102*, 9750.
(27) Quindt, V.; Saurenz, D.; Schmitt, O.; Schär, M.; Dezember, T.; Wolmershäuser, G.; Sitzmann, H. *J. Organomet. Chem.* **1999**, *579*, 376.
(28) Burns, C. T.; Shapiro, P. J.; Budzelaar, P. H. M.; Willet, R.; Vij, A. *Organometallics* **2000**, *19*, 3361.

Table 1. Crystal Data and Structure Refinement for $[Cp^*_2Al][AlCl_4]$

empirical formula	$C_{20}H_{30}Al_2Cl_4$
formula weight	466.20
temperature	153(2) K
wavelength	0.71069 Å
crystal system, space group	triclinic, *P*-1
unit cell dimensions	$a = 7.7548$ (1), $\alpha = 85.7100(7)°$ $b = 17.3747(3)$, $\beta = 83.6011(8)°$ $c = 18.0806(4)$, $\gamma = 84.7879(7)°$
volume	2405.79(7) A^3
Z, calculated density	4, 1.287 g/cm^3
absorption coefficient	0.568 mm^{-1}
F(000)	976
crystal size	0.4 × 0.4 × 0.3 mm
θ range for data collection	2.99−25.06°
limiting indices	$-9 \le h \le 9$, $-18 \le k \le 20$, $-21 \le l \le 20$
reflections collected/unique	32 448/8499 [$R_{(int)} = 0.0411$]
refinement method	full-matrix least-squares on F^2
data/restraints/parameters	8499/0/489
goodness-of-fit on F^2	1.021
final *R* indices [$I > 2\sigma(I)$]	$R_1 = 0.0465$, w$R_2 = 0.1097$
R indices (all data)	$R_1 = 0.0703$, w$R_2 = 0.1219$
largest diff. peak and hole	0.971 and −0.754 e Å^{-3}

solution of Cp^*_2AlCl (1.00 g, 3.00 mmol) in CH_2Cl_2 (40 mL) at −78 °C. After being warmed to room temperature, the resulting amber solution was allowed to stir for 14 h. The solution was concentrated to a volume of 10 mL and cooled to −20 °C to afford a crop of colorless block-shaped crystals (1.3 g, 92.8%), mp 123−124 °C (decomp). LRMS: 464 ($Cp^*_2Al_2Cl_4$, 3%), 429 ($Cp^*_2Al_2Cl_3$, 60%), 329 ($Cp^*Al_2Cl_4$, 7%), 297 (Cp^*_2Al, 20%), 197 (Cp^*AlCl, 100%), 137 (Cp^*H_2, 55%). HRMS: calcd for $C_{20}H_{30}Al_2Cl_4$, 464.0732; found, 464.0743. HRMS: calcd for $C_{20}H_{30}Al$, 297.2163; found, 297.2166. ^{1}H NMR (300.19 MHz, CD_2Cl_2): δ 2.187 (s, C_5Me_5). ^{27}Al NMR (78.31 MHz, CD_2Cl_2): δ −102.92 (s, $(\eta^5\text{-}C_5Me_5C_5)_2Al^+$), δ 115.215 (s, $AlCl_4^-$).

X-ray Crystallography. A crystal of $[Cp^*_2Al][AlCl_4]$ was covered in perfluoro(poly)ether, mounted on a goniometer head, and rapidly placed into the −120 °C stream of dry nitrogen of an Oxford Cryostream low-temperature device. The data were collected on a Nonius Kappa CCD diffractometer using a graphite monochromator with Mo Kα radiation ($\lambda = 0.71073$ Å). A total of 280 frames of data were collected using ω-scans with a scan range of 1.9° and a counting time of 38 s per frame. A summary of the collection, solution, and refinement data is presented in Table 1. Data reduction was performed using DENZO-SMN.[29] The structure was solved by direct methods using SIR92[30] and refined by full-matrix least-squares on F^2 with anisotropic displacement parameters for the non-H atoms using SHELXL-93.[31] The function minimized was $R_w(F_o^2) = \{\sum[w(F_o^2 - F_c^2)^2/\sum[w(F_o^2)^2]^{1/2}$. The hydrogen atoms were placed in geometrically calculated positions and were refined using a riding model and a general isotropic thermal parameter.

Solid-State NMR Spectroscopy. Samples were carefully powdered under an inert atmosphere and packed tightly into 4 mm o.d. rotors. Solid-state MAS and static NMR spectra were obtained on a 9.4 T (^{1}H = 400 MHz) wide bore Bruker AMX-400 NMR spectrometer at Dalhousie University, operating at $\upsilon_0(^{27}Al) = 104.26$ MHz. Additional spectra were acquired on a Varian Infinity Plus NMR spectrometer and Oxford 9.4 T magnet at the University of Windsor, at similar operating frequencies. Aluminum-27 chemical shifts were referenced to a 1.0 M solution of $Al(NO_3)_3$ ($\delta_{iso} = 0$ ppm). A Bruker 4 mm triple-resonance MAS NMR probe was used for the acquisition of both static and MAS spectra, with typical MAS spinning speeds of $\upsilon_{rot} = 6.26$ and 8.00 kHz. Bloch decay experiments were performed with high-power proton decoupling ($\upsilon_2 = 62.5$ kHz). Pulse widths of 1.8 and 5.0 μs were applied in the static and MAS ^{27}Al experiments, respectively, both with $\upsilon_1 = 50$ kHz. For MAS experiments, 1000−2000 transients were collected, and for static experiments, ca. 45 000 scans were acquired. The ^{27}Al SATRAS NMR spectrum was acquired at a spinning speed $\upsilon_{rot} = 6000$ Hz using a pulse width of 0.6 μs and an rf field $\upsilon_1 = 86$ kHz. A total of 12 916 transients were collected using a 3.0 s pulse delay and high-power proton decoupling. The MAS speed was chosen very carefully to prevent overlap of peaks from different aluminum sites. Processed spectra were baseline corrected using NUTS NMR processing software.

Carbon-13 single-pulse and cross-polarization (CP) MAS NMR experiments were conducted using the same spectrometers as above, operating at $\upsilon_0(^{13}C) = 100.51$ MHz, and with high-power proton decoupling during acquisition. ^{13}C NMR spectra were referenced to TMS ($\delta_{iso}(^{13}C) = 0.0$ ppm) by setting the high-frequency resonance of adamantane to 38.57 ppm. Spectra were acquired at two different spinning speeds (2000 and 4723 Hz) with a 3.5 μs pulse width and $\upsilon_1 = 71.4$ kHz rf field.

Spectral Simulations. Analytical simulations of the ^{27}Al NMR spectra were carried out on a Pentium III computer using the WSOLIDS simulation package by Dr. Klaus Eichele, which was developed in Prof. Wasylishen's laboratory at Dalhousie University. This software incorporates the space-tiling method of Alderman and co-workers for the generation of frequency domain solid-state NMR powder patterns.[32] Carbon shielding tensors were extracted from ^{13}C MAS NMR spectra using the method of Herzfeld and Berger.[33]

The SIMPSON[34] software package for general simulations of solid-state NMR spectra was used to simulate the ^{27}Al MAS NMR central and satellite transitions of $[Cp^*_2Al][AlCl_4]$. Simulations were accomplished by the *gcompute* method of powder averaging using the *zcw4180* crystal file provided in the package and a spectral width of 600 kHz. The start and detect operators were set to I_{1x} and I_{1p}, respectively, requiring us only to set the delay parameter to 9999 μs in the pulse sequence section. Simulated spectra were saved in free induction decay (FID) format as ASCII files without any mathematical manipulation and converted to NUTS readable files using a small script written within our research group.

Theoretical Methods. Ab initio calculations were conducted using the Gaussian 98 program suite[35] on a Dell Precision 420 dual-733 MHz Pentium III computer. CS tensors for the D_{5d} and D_{5h} aluminocenium cation were calculated using the GIAO method[36] with the 6-31G** and 6-311G** basis sets using RHF and B3LYP methods (Becke's three parameter hybrid[37] and the correlation functional of Lee, Yang, and Parr[38]). There is no established absolute chemical shielding scale

(29) DENZO-SMN. Otwinowski, Z.; Minor, W. In *Methods in Enzymology*, **276**: Macromolecular Crystallography, part A, 307 B 326; Carter, C. W., Jr., Sweets, R. M., Eds.; Academic Press: New York, 1997.
(30) Altomare, A.; Cascarano, G.; Giacovazzo, C.; Guagliardi, A. *SIR92*. A Program for Crystal Structure Solution. *J. Appl. Crystallogr.* **1993**, *26*, 343−350.
(31) Sheldrick, G. M. *SHELXL93*. Program for the Refinement of Crystal Structures; University of Gottingen: Germany, 1993.
(32) Alderman, D. W.; Solum, M. S.; Grant, D. M. *J. Chem. Phys.* **1986**, *84*, 3717.
(33) (a) Herzfeld, J.; Berger, A. E. *J. Chem. Phys.* **1980**, *73*, 6021. (b) Maricq, M. M.; Waugh, J. S. *J. Chem. Phys.* **1979**, *70*, 3300.
(34) Bak, M.; Rasmussen, J. T.; Nielsen, N. C. *J. Magn. Reson.* **2000**, *147*, 296.
(35) Frisch, M. J.; Trucks, G. W.; Schlegel, H. B.; Scuseria, G. E.; Robb, M. A.; Cheeseman, J. R.; Zakrzewski, V. G.; Montgomery, J. A., Jr.; Stratmann, R. E.; Burant, J. C.; Dapprich, S.; Millam, J. M.; Daniels, A. D.; Kudin, K. N.; Strain, M. C.; Farkas, O.; Tomasi, J.; Barone, V.; Cossi, M.; Cammi, R.; Mennucci, B.; Pomelli, C.; Adamo, C.; Clifford, S.; Ochterski, J.; Petersson, G. A.; Ayala, P. Y.; Cui, Q.; Morokuma, K.; Malick, D. K.; Rabuck, A. D.; Raghavachari, K.; Foresman, J. B.; Cioslowski, J.; Ortiz, J. V.; Baboul, A. G.; Stefanov, B. B.; Liu, G.; Liashenko, A.; Piskorz, P.; Komaromi, I.; Gomperts, R.; Martin, R. L.; Fox, D. J.; Keith, T.; Al-Laham, M. A.; Peng, C. Y.; Nanayakkara, A.; Challacombe, M.; Gill, P. M. W.; Johnson, B.; Chen, W.; Wong, M. W.; Andres, J. L.; Gonzalez, C.; Head-Gordon, M.; Replogle, E. S.; Pople, J. A. *Gaussian 98*, revision A.9; Gaussian, Inc.: Pittsburgh, PA, 1998.
(36) (a) Ditchfield, R. *Mol. Phys.* **1974**, *27*, 789. (b) Wolinski, K.; Hinton, J. F.; Pulay, P. *J. Am. Chem. Soc.* **1990**, *112*, 8251 and references therein.
(37) (a) Becke, A. D. *J. Chem. Phys.* **1993**, *98*, 5648. (b) Becke, A. D. *Phys. Rev. A* **1988**, *38*, 3098.
(38) Lee, C.; Yang, W.; Parr, R. G. *Phys. Rev. B* **1988**, *37*, 785.

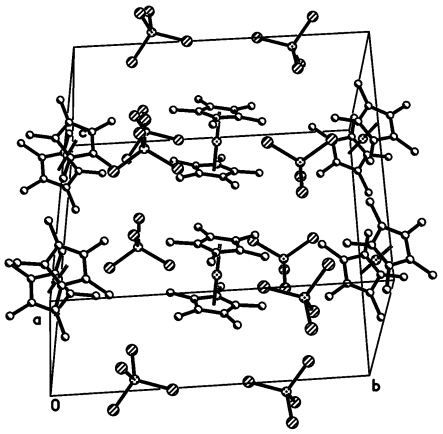

Figure 1. The unit cell for $[Cp^*_2Al][AlCl_4]$ (see Table 1 for parameters).

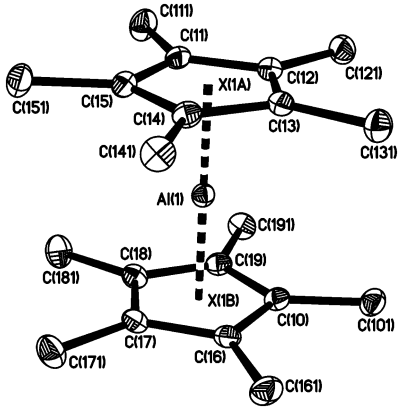

Figure 2. Structure of the $[Cp^*_2Al]^+$ cation with D_{5d} symmetry. Hydrogen atoms are omitted for clarity.

for ^{27}Al; thus, calculated ^{27}Al chemical shifts were referenced with respect to the $Al(H_2O)_6^{3+}$ cation. The absolute chemical shielding for $Al(H_2O)_6^{3+}$ was calculated using both the RHF and the B3LYP methods with both the 6-31G** and the 6-311G** basis sets. Because the isotropic chemical shift of $Al(H_2O)_6^{3+}$ (aq) is set to 0.0 ppm,[39] the chemical shifts of the molecules could be calculated as $\delta = \sigma_{ref} - \sigma_{sample}$. Calculated EFG components were converted from atomic units (au) to MHz [40] by multiplying the largest component of the EFG tensor, V_{33}, by $eQ/h \times 9.7177 \times 10^{21}$ V m^{-2}, where $Q(^{27}Al) = 1.403 \times 10^{-29}$ m^2 (ref 19) and $e = 1.602 \times 10^{-19}$ C. Calculations of carbon shielding tensors were carried out using both RHF and B3LYP methods, with 6-31G** and 6-311G** basis sets. Carbon chemical shielding parameters were converted to carbon chemical shifts by calculating the absolute chemical shielding of the carbon nucleus in CO and by setting the chemical shift to its experimentally determined value of $\delta_{iso}(^{13}C) = 187.1$ ppm with respect to the carbon nucleus in TMS ($\delta_{iso}(^{13}C) = 0.0$ ppm).[41]

Theoretical contributions to aluminum chemical shielding due to mixing of molecular orbitals were calculated for $[Cp^*_2Al]^+$, $Al(H_2O)_6^{3+}$, and $AlCl_4^-$ using the Amsterdam density functional software package version 2000.02 (ADF2000.02).[42] Pure exchange was used for the local density approximation (LDA), and Becke's[37] exchange with the Lee−Yang−Parr[38] correlation functionals were applied for the generalized gradient approximation (GGA). Calculations were performed on crystal structure molecular coordinates using the all-electron ADF standard basis set *V*, which is a triple-ζ basis set with two polarization functions for H−Ar.

Simulations of ^{13}C powder patterns affected by molecular motion were done using a custom-written C++ chemical exchange program. Calculations were carried out on a Dell Precision 420 dual-733 MHz Parallel Pentium III computer. Hemispherical ZCW angle sets were used for powder averaging,[43] and inversion and diagonalization routines for square matrixes were performed with release 3.0 of the LAPACK linear algebra package.[44]

Results and Discussion

X-ray Crystal Structure of $[Cp^*_2Al][AlCl_4]$. The unit cell for the X-ray crystal structure of $[Cp^*_2Al][AlCl_4]$ is depicted in Figure 1, with the summary of pertinent X-ray data given in Table 1. The $[Cp^*_2Al][AlCl_4]$ salt crystallizes in the space group $P\bar{1}$ and features four asymmetric units per unit cell. There are two crystallographically nonequivalent $[Cp^*_2Al]^+$ cations in the unit cell. However, the structures of both cations are very similar, and each cation possesses almost perfect D_{5d} symmetry due to the staggering of the Cp* rings. The structure of one such cation, which is virtually identical to those found in other decamethylaluminocenium salts,[28,45] is shown in Figure 2. The tetrachloroaluminate anions are only slightly distorted from ideal tetrahedral symmetry and there are no unusually short contacts between the chlorine atoms of the tetrachloroaluminate anions and the decamethylaluminocenium cations.

Solid-State ^{27}Al NMR Studies. The ^{27}Al MAS NMR spectrum of $[Cp^*_2Al][AlCl_4]$ reveals three different aluminum-containing species (Figure 3A). The normal range of ^{27}Al chemical shifts falls between $\delta_{iso}(^{27}Al)$ ca. 0 ppm for hexacoordinate aluminum and $\delta_{iso}(^{27}Al)$ ca. 100 ppm for tetracoordinate aluminum.[20,46] Accordingly, the peak at 101.0 ppm, with a line width of ca. 80 Hz (without any apodization of the FID), is assigned to the $[AlCl_4]^-$ anions. This peak is expected to be relatively narrow, because the quadrupolar interaction in a pseudotetrahedral environment is relatively small due to the high spherical symmetry.

Expansion of the low-frequency portion of the spectrum (Figure 3B) reveals two sharp resonances arising from the two crystallographically nonequivalent $[Cp^*_2Al]^+$ cations in the unit cell, with slightly different chemical shifts of −115.3 and −117.0 ppm, and slightly different line widths ($\Delta\nu_{1/2} = 80$ and 70 Hz, respectively). These shifts are similar to those measured in solution ^{27}Al NMR experiments on $[Cp^*_2Al]^+$ and fall well outside of the usual aluminum chemical shift range. There is no visible second-order quadrupolar powder pattern for these peaks; however, C_Q is nonzero because there is evidence of spinning sidebands resulting from satellite transitions observed in the spectra (full analysis of the ^{27}Al powder pattern is discussed at the end of this section of the paper). The EFG at the aluminum nucleus must be small because of the high symmetry of the $[Cp^*_2Al]^+$ cations (vide infra) and possibly because of rapid rotation of the Cp* rings at room temperature.

(39) Nöth, H. *Z. Naturforsch.* **1980**, *35b*, 119.
(40) (a) Brown, R. D.; Head-Gordon, M. P. *Mol. Phys.* **1987**, *61*, 1183. (b) Cummins, P. L.; Bacskay, G. B.; Hush, N. S. *Mol. Phys.* **1987**, *62*, 193.
(41) Jameson, A. K.; Jameson, C. J. *Chem. Phys. Lett.* **1987**, *134*, 461.
(42) (a) Schreckenbach, G.; Ziegler, T. *J. Phys. Chem.* **1995**, *99*, 606. (b) Patchkovskii, S.; Ziegler, T. *J. Phys. Chem. A* **2001**, *105*, 5490. (c) *ADF User*'s *Guide*, *ADF Program System Release 2000.02*.
(43) Eden, M.; Levitt, M. H. *J. Magn. Reson.* **1998**, *132*, 220.
(44) LAPACK is a Fortran 77 library providing routines for solving linear algebra problems. Code is available at http://www.netlib.org/lapack.
(45) (a) Dohmeier, C.; Schnöckel, H.; Robl, C.; Schneider, U.; Alrichs, R. *Angew. Chem., Int. Ed. Engl.* **1993**, *32*, 1655. (b) Uffing, C.; Ecker, A.; Baum, E.; Schnöckel, H. *Z. Anorg. Allg. Chem.* **1999**, *625*, 1354. (c) Dohmeier, C.; Baum, E.; Ecker, A.; Koppe, R.; Schnöckel, H. *Organometallics* **1996**, *15*, 4702. (d) Burns, C. T.; Stelck, D. S.; Shapiro, P. J.; Vij, A.; Kunz, K.; Kehr, G.; Concolino, T.; Rheingold, A. L. *Organometallics* **1999**, *18*, 5432.
(46) *Multinuclear NMR*; Akitt, J. W., Mason, J., Eds.; Plenum Press: New York, 1987.

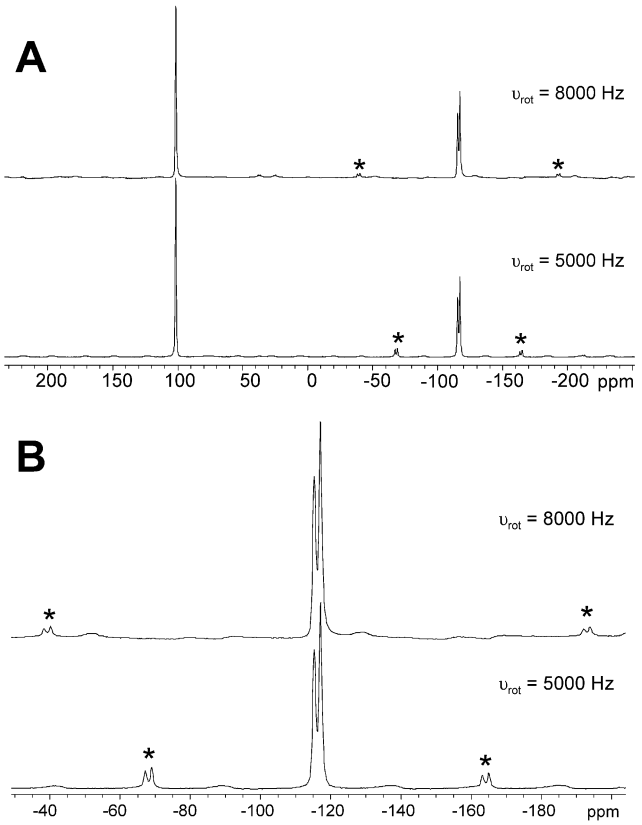

Figure 3. (A) ^{27}Al MAS NMR spectra of $[Cp^*_2Al][AlCl_4]$ at 9.4 T. Asterisks denote spinning sidebands. (B) Close-up of $[Cp^*_2Al]^+$ resonance.

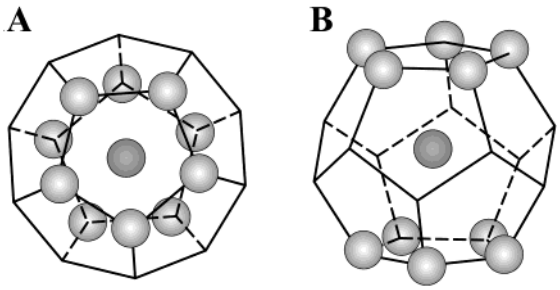

Figure 4. Top view (A) and side view (B) of the arrangement of the aluminocenium cation structure in a centrosymmetric dodecahedron, with Al at the center, and carbon atoms located on 10 of the 20 vertices.

The geometrical shape of the aluminocenium cation can be visualized as a centrosymmetric dodecahedron which has 12 sides and 20 vertices (Figure 4), with the aluminum at the center and each of the 10 Cp* ring carbons sitting at the two sets of five pentagonally arranged vertices. The remaining 10 vertices zigzag about the equator of the molecule. It has been demonstrated for centrosymmetric polyhedra that there should be a zero EFG at the centrosymmetric point, S_0, if $V/2$ equal charges are distributed among V vertices in such a way that no two charges are related by reflection through S_0.[47,48] Of course, the decamethylaluminocenium cation does not perfectly fit onto the vertices of a centrosymmetric dodecahedron, accounting for some presence of a nonzero EFG tensor at the aluminum nucleus. The combination of this arrangement of carbon atoms about the aluminum atom and rapid rotation of the Cp* rings

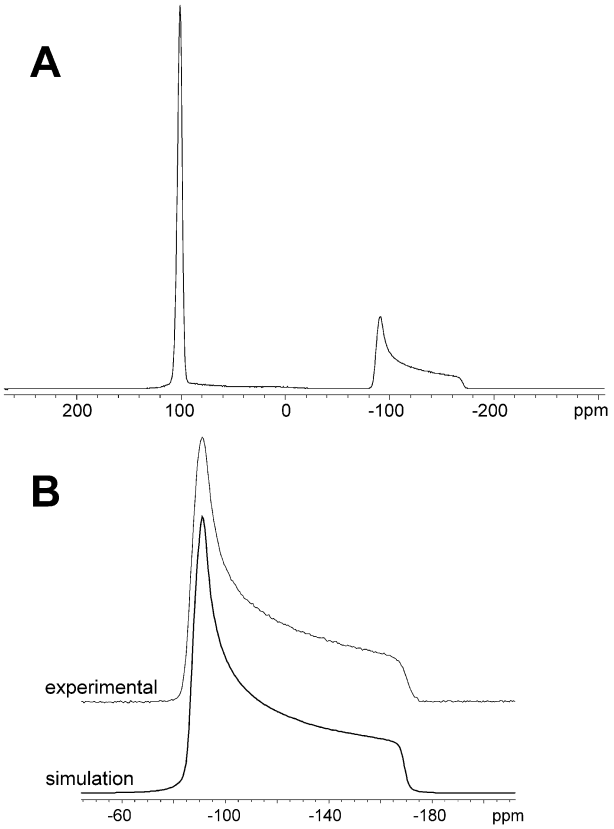

Figure 5. (A) Static ^{27}Al NMR spectrum of $[Cp^*_2Al][AlCl_4]$ at 9.4 T. (B) Experimental (top) and calculated (bottom) ^{27}Al CSA patterns of $[Cp^*_2Al][AlCl_4]$ at 9.4 T. Parameters are discussed in the main text.

at ambient temperatures (which normally serve to reduce nuclear quadrupole coupling constants)[49] results in a very small aluminum nuclear quadrupole interaction.

Initially, one might suspect that if the ^{27}Al quadrupolar interaction is small for a molecule of this relatively high symmetry, the degree of anisotropic chemical shielding must also be very small. However, on the basis of a superficial examination of the symmetry and structure of this molecule, it becomes very apparent that the chemical shielding along the C_5 axis of the molecule must be different from shielding perpendicular to this axis. Not surprisingly, the aluminum chemical shielding anisotropy in the $[Cp^*_2Al]^+$ cation is substantial. The static ^{27}Al NMR spectrum (Figure 5A) reveals a classical CSA powder pattern for the $[Cp^*_2Al]^+$ aluminum nucleus which spans approximately 83 ppm, and a broad relatively symmetric peak centered at ca. 101 ppm corresponding to the $[AlCl_4]^-$ anions. Shielding patterns similar to that of the $[Cp^*_2Al]^+$ cation are rarely observed for quadrupolar nuclei with sizable quadrupole moments because static powder patterns are typically influenced by both anisotropic quadrupolar and chemical shielding interactions, as well as their relative orientation.[50,51]

Spectral simulations of the static pattern of the aluminocenium cation (Figure 5B) reveal an almost axially symmetric chemical shielding tensor with the following principal components: $\delta_{11} = -87(1)$, $\delta_{22} = -92(1)$, and $\delta_{33} = -170(1)$ ppm, which

(47) (a) Knop, O.; Palmer, E. M.; Robinson, R. W. *Acta Crystallogr., Sect. A* **1975**, *31*, 19. (b) Knop, O. *Acta Crystallogr., Sect. A* **1976**, *32*, 147.
(48) Akitt, J. W.; McDonald, W. S. *J. Magn. Reson.* **1984**, *58*, 401.
(49) Lucken, E. A. C. *Nuclear Quadrupole Coupling Constants*; Academic Press: New York, 1969.
(50) Cheng, J. T.; Edwards, J. C.; Ellis, P. D. *J. Phys. Chem.* **1990**, *94*, 553.
(51) Power, W. P.; Wasylishen, R. E.; Mooibroek, S.; Pettitt, B. A.; Danchura, W. *J. Phys. Chem.* **1990**, *94*, 591.

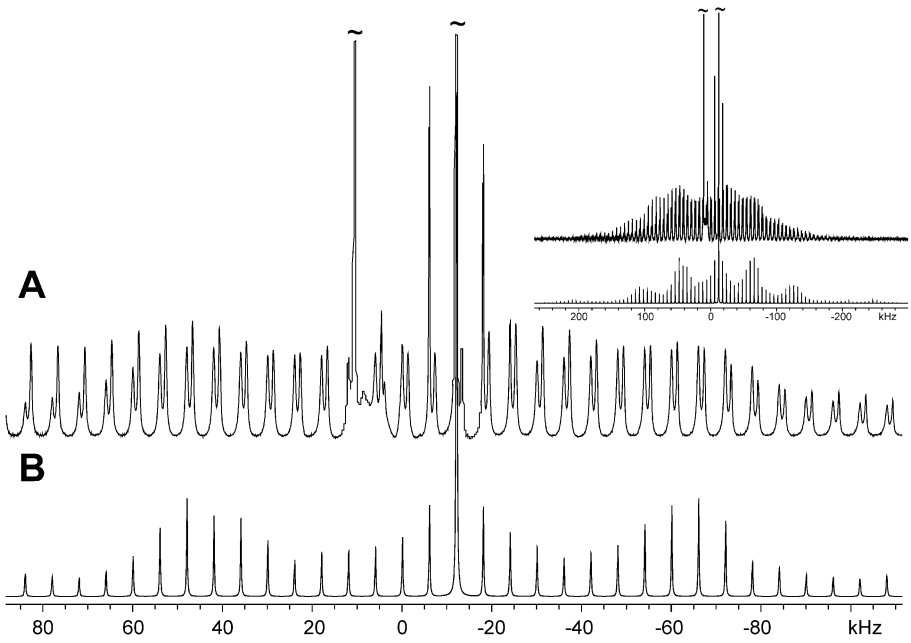

Figure 6. Experimental (A) and simulated (B) (with SIMPSON) ^{27}Al SATRAS NMR spectra of $[Cp^*_2Al][AlCl_4]$ at 9.4 T. Inset: Full satellite transition pattern.

correspond to $\delta_{iso} = -116.3(7)$ ppm, $\Omega = 83(3)$ ppm, and $\kappa = 0.88(3)$. This is the largest aluminum CSA measured by solid-state NMR to date. The static CSA pattern results from the overlap of two indistinguishable CSA patterns with very similar isotropic chemical shifts; consequently, two separate shielding tensors cannot be extracted by simulation of the static spectrum. The axial symmetry of the tensor can be immediately correlated to the high symmetry of the molecule: the most shielded principal component, δ_{33}, is oriented along the C_5 axis of the molecule, with the other two components oriented perpendicular to this axis.

The full ^{27}Al NMR spectrum including central and satellite transitions is displayed in Figure 6. The pattern is extremely complex due to overlap of satellite transition spinning sidebands from the different aluminum sites. Additionally, the overall shape of the pattern and exact position and intensity of each spinning sideband are dependent upon both the anisotropic chemical shielding and the quadrupolar parameters.[52] Careful simulation of the full ^{27}Al central and satellite transition patterns of the $[Cp^*_2Al]^+$ cation, including the chemical shielding tensor parameters obtained from analysis of the static ^{27}Al NMR powder pattern, allows for the determination of $C_Q(^{27}Al) = 0.86(10)$ MHz and $\eta_Q = 0.0$.

On a final note, there is some broadening in the peak corresponding to the tetrahedral $[AlCl_4]^-$ sites which may be attributed to a variety of sources, including two magnetically nonequivalent $[AlCl_4]^-$ anions with slightly different chemical shifts, a pseudotetrahedral anionic structure giving rise to a noticeable anisotropic quadrupolar interaction (the large spinning sideband manifold associated with the $[AlCl_4]^-$ sites indicates that there is definitely a nonzero C_Q), or perhaps unaveraged dipolar coupling with the chlorine atoms in the anion.

Solid-State ^{13}C NMR Studies. Examination of the ^{13}C CPMAS NMR spectra (Figure 7) reveals two types of carbon sites: the Cp* ring carbons at 118.7 ppm and the Cp* methyl carbons at 10.4 ppm. Sharp transitions for the isotropic chemical shifts and their spinning sideband manifolds imply magnetic equivalence of all of the carbon sites, which is only possible if dynamic exchange of carbons is occurring as the result of ring motion. The Cp* aromatic carbons are observed to have a significant carbon chemical shielding anisotropy with axial CS tensors, with $\Omega = 108(2)$ ppm and $\kappa = 1.0(5)$, corresponding to $\delta_{11} = 154.7$, $\delta_{22} = 154.7$, and $\delta_{33} = 46.7$ ppm. This is comparable to ^{13}C chemical shielding tensors that were previously measured in Cp_2Mg and related complexes.[7,8] The axial symmetry of the CS tensor is believed to arise from rapid rotation of the Cp* rings − this aspect of ring dynamics is further discussed in the theoretical section of this paper.

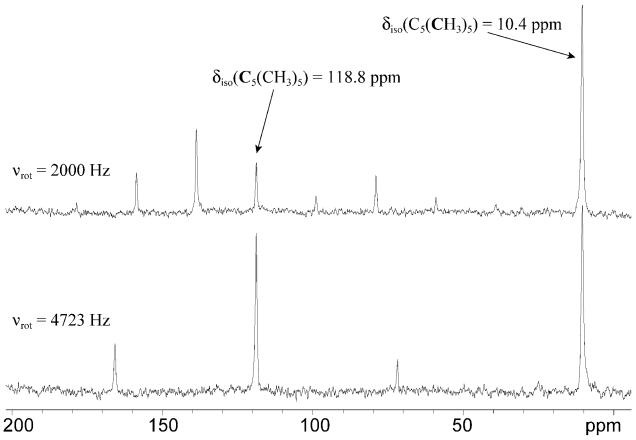

Figure 7. Carbon-13 CPMAS NMR of $[Cp^*_2Al][AlCl_4]$ at 9.4 T.

A Theoretical Study of Aluminum Chemical Shielding and EFG Tensors in $[Cp^*_2Al]^+$. In the past five years, both main group and transition metal metallocenes have been the subject of a number of theoretical studies, including general theory of structure and bonding in metallocenes,[53,54] and chemical shield-

(52) Jäger, C. *NMR: Basic Princ. Prog.* **1994**, *31*, 133.

(53) Sapunov, V. N.; Kirchener, K.; Schimd, R. *Coord. Chem. Rev.* **2001**, *214*, 143.

(54) Kwon, O.; McKee, M. L. *J. Phys. Chem. A* **2001**, *105*, 10133.

Table 2. Experimental and Theoretical Aluminum Electric Field Gradient Tensors

	V_{11} (au)	V_{22} (au)	V_{33} (au)	$\lvert C_Q \rvert$ (MHz)[a]	η_Q	SCF energy (au)
experimental	n.a.	n.a.	n.a.	0.86(10)	0.0	n.a.
D_{5d} − staggered						
RHF/6-31G**	−0.005826	−0.005826	0.011652	0.38	0.0	−1016.61056897
RHF/6-311G**	0.010641	0.010641	−0.021282	0.70	0.0	−1016.75137056
B3LYP/6-31G**	0.021950	0.021950	−0.043900	1.44	0.0	−1022.50615250
B3LYP/6-311G**	0.022903	0.022903	−0.045805	1.51	0.0	−1022.66892738
D_{5h} − eclipsed						
RHF/6-31G**	−0.003235	−0.003235	0.006469	0.21	0.0	−1016.59933705
RHF/6-311G**	0.009193	0.009193	−0.018386	0.61	0.0	−1016.74005616
B3LYP/6-31G**	0.026867	0.026867	−0.053734	1.77	0.0	−1022.49730276
B3LYP/6-311G**	0.029157	0.029157	−0.058313	1.92	0.0	−1022.66040230

[a] Calculated EFG tensors were converted from atomic units (au) to MHz by multiplying the largest component of the EFG tensor, V_{33}, by $eQ/h \times 9.7177 \times 10^{21}$ V m^{-2}, where $Q(^{27}\text{Al}) = 1.403 \times 10^{-29}$ m^2 (ref 19) and $e = 1.602 \times 10^{-19}$ C.

ing and electric field gradient tensors in ferrocene.[55,56] The central metal nuclei in metallocenes can be placed into a plethora of different symmetries, geometries, and chemical bonding situations, thereby providing NMR spectroscopists with the ideal arena to probe the origins of chemical shielding for many different metal nuclei. It is also important to correlate the chemistry and structure of metallocenes with anisotropic NMR interaction tensors, as this has great potential for identifying precursors and byproducts of catalysis in disordered systems, studying metallocene reactivity and transition states, and probing intermolecular and intramolecular dynamics and chemical exchange mechanisms in metallocenes.

Calculations of NMR interaction tensors, including chemical shielding, *J*-coupling, and electric field gradient tensors, using ab initio SCF methods or density functional theory are abundant in the current literature and represent a formidable challenge to theoreticians.[57,58] The EFG tensor is a first-order property and can be calculated from the ground-state wave function of a molecule. Ab initio RHF and DFT calculations should, in theory, provide very accurate values of the quadrupolar coupling constant. However, there are a number of factors prohibiting accurate calculations of quadrupolar parameters including limited basis set sizes, electron correlation, and relativistic effects. Perhaps more significantly, EFG tensors measured in the solid state will often differ greatly from those calculated on gas-phase or computationally geometry-optimized structures, because it is difficult to account for long-range electrostatic interactions with neighboring molecules and/or the solid lattice, as well as the effects of inter- and intramolecular motion (which are influenced by temperature changes),[49] on the characteristics of the EFG tensor.

Calculations of the ^{27}Al EFG tensor at the aluminum nucleus in the isolated D_{5d} $[Cp^*_2Al]^+$ cation are summarized in Table 2. There is not very good agreement between the experimentally determined values of $C_Q(^{27}\text{Al})$ and either RHF or B3LYP results. RHF calculations seem to approach the experimental value of C_Q as the basis set increases in size, whereas the B3LYP calculations consistently overestimate C_Q. In all cases, an axially symmetric EFG tensor is predicted, in good agreement with our experimental results. The EFG tensor orientation is pictured in Figure 8A, with the largest (and unique) component of the EFG along the C_5 symmetry axis. The lack of accuracy of these calculations may stem from the reasons discussed above, with the largest discrepancies perhaps arising from motion of Cp* rings.

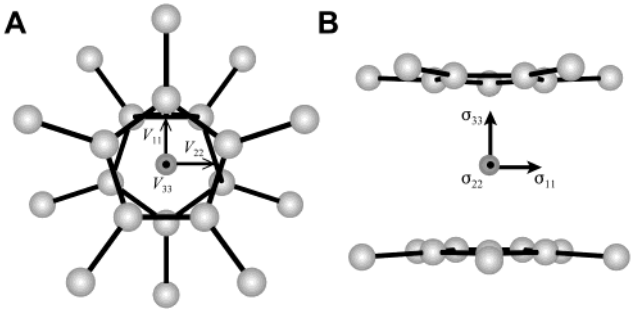

Figure 8. The orientation of the (A) electric field gradient and (B) chemical shielding tensors in $[Cp^*_2Al]^+$, as determined by RHF calculations with the 6-31G** basis set. Hydrogen atoms are omitted for clarity.

Chemical shielding is a second-order property and is dependent upon both the ground-state wave function and the orientation-dependent symmetry-allowed mixing of ground- and excited-state molecular orbitals (i.e., chemical shielding is dependent upon how the ground-state wave function changes in the presence of an external magnetic field). Under the Ramsey formalism, there are two contributions to nuclear magnetic shielding: diamagnetic shielding and paramagnetic shielding. Diamagnetic shielding, which is responsible for magnetically shielding the nucleus from the applied magnetic field (i.e., a negative frequency shift), arises from induced circulation of electrons in ground-state molecular orbitals and can be calculated with relative ease. Paramagnetic shielding, which is most often associated with magnetic deshielding of the nucleus (i.e., positive frequency shift), arises from two sources: (i) the major contribution is usually magnetic-dipole-allowed mixing of ground- and excited-state molecular orbitals, and (ii) there is a minor contribution from mixing of occupied molecular orbitals. The diamagnetic and paramagnetic contributions cannot be distinguished experimentally by NMR spectroscopy; however, careful analysis of orientation-dependent diamagnetic and paramagnetic shielding contributions often helps to elucidate the origin of chemical shielding and its relation to molecular structure.

We have conducted a series of computations of anisotropic NMR shielding tensors using RHF, hybrid RHF/DFT, and pure DFT methods to (i) determine the theoretical ^{27}Al chemical

(55) Schreckenbach, G. *J. Chem. Phys.* **1999**, *110*, 11936.
(56) Schwerdtfeger, P.; Söhnel, T.; Pernpointner, M.; Laerdahl, J. K.; Wagner, F. E. *J. Chem. Phys.* **2001**, *115*, 5913.
(57) (a) Helgaker, T.; Jaszuński, M.; Ruud, K. *Chem. Rev.* **1999**, *99*, 293. (b) Buhl, M.; Kaupp, M.; Malkina, O. L.; Malkin, V. G. *J. Comput. Chem.* **1999**, *20*, 91. (c) Jameson, C. J. *Annu. Rev. Phys. Chem.* **1996**, *47*, 135. (d) de Dios, A. C. *Prog. Nucl. Magn. Reson. Spectrosc.* **1996**, *29*, 229.
(58) (a) Fukui, H. *Prog. Nucl. Magn. Reson. Spectrosc.* **1999**, *35*, 267. (b) Contreras, R. H.; Peralta, J. E.; Giribet, C. G.; De Azua, M. C.; Facelli, J. C. *Annu. Rep. NMR Spectrosc.* **2000**, *41*, 55.

Table 3. Experimental and Theoretical Aluminum Chemical Shift Tensors in the Decamethylaluminocenium Cation[a]

	δ_{11} (ppm)	δ_{22} (ppm)	δ_{33} (ppm)	δ_{iso} (ppm)[b]	Ω (ppm)	κ
experimental	−87(1)	−92(1)	−170(1)	−116.3(7)	83(3)	0.88(3)
D_{5d} − staggered						
RHF/6-31G**	−86.52	−86.52	−157.85	−110.30	71.33	1.00
RHF/6-311G**	−102.06	−102.06	−172.49	−125.54	70.44	1.00
B3LYP/6-31G**	−74.60	−74.95	−156.11	−101.89	81.50	0.99
B3LYP/6-311G**	−93.46	−93.66	−180.33	−122.48	86.87	1.00
D_{5h} − eclipsed						
RHF/6-31G**	−105.26	−105.26	−150.92	−120.48	45.66	1.00
RHF/6-311G**	−119.68	−119.68	−168.50	−135.96	48.82	1.00
B3LYP/6-31G**	−95.74	−96.41	−144.01	−112.05	48.27	0.97
B3LYP/6-311G**	−113.87	−114.12	−171.65	−133.21	57.78	0.99

[a] Absolute chemical shieldings are converted to chemical shifts with the formula $\sigma_{ref} - \sigma_{sample}$, where σ_{ref} is the absolute chemical shielding of the hexacoordinate $Al(H_2O)_6^{3+}$ cation. See Experimental Section for details. [b] $\delta_{iso} = (\delta_{11} + \delta_{22} + \delta_{33})/3$, $\Omega = \delta_{11} - \delta_{33}$, and $\kappa = 3(\delta_{22} - \delta_{iso})/\Omega$.

shielding tensor components for comparison with experimental values, while examining the diamagnetic and paramagnetic chemical shielding contributions, (ii) examine the orientation of the CS tensor with respect to the molecular frame and the EFG tensor, (iii) determine the barrier to rotation of the Cp* rings, while comparing aluminum CS tensors for different rotational isomers, and (iv) calculate the contributions from mixing of individual orbitals to diamagnetic and paramagnetic shielding (using the ADF software package).

Experimental and theoretical chemical shift tensors are compared in Table 3 (the absolute chemical shielding values have been converted to the aluminum chemical shift scale, as described in the Experimental Section of this paper). Both RHF and B3LYP calculations on the D_{5d} $[Cp^*_2Al]^+$ cation correspond very closely with experimental results, with the RHF calculations slightly underestimating Ω, and calculations with the larger 6-311G** basis set overestimating the isotropic chemical shift. In all cases, an axially symmetric chemical shielding tensor is predicted (i.e., $\kappa = 1.0$, so $\delta_{11} = \delta_{22}$ and δ_{33} is the unique component). The orientation of the aluminum CS tensor is similar to that of the EFG tensor, with the most shielded component, δ_{33}, oriented along the C_5 symmetry axis of the molecule (Figure 8B). Interestingly, calculations on the D_{5h} $[Cp^*_2Al]^+$ cation, in which the Cp* rings are eclipsed, indicate that the span of the aluminum chemical shielding tensor decreases (by ca. 25−30 ppm) in this rotational conformation. This suggests that at room temperature, if the barrier to rotation for the Cp* rings is small enough, we may be observing an average aluminum chemical shielding tensor.

In Figure 9, theoretically calculated rotational barriers are pictured for the $[Cp^*_2Al]^+$ cation. Initial calculations of the rotational barrier involved changing the relative orientation of the Cp* rings by adjusting the position of one ring. B3LYP calculations with both the 6-31G** and the 6-311G** basis sets displayed an unusual discontinuity for the staggered D_{5d} species (energies for different conformers are signified by rectangular and circular points), making it apparent that it was necessary to conduct a geometry optimization for each rotational conformer. A rotational barrier of 4.15 kJ mol^{-1} was calculated from B3LYP/6-311G** geometry optimizations, with the staggered D_{5d} conformation possessing the lowest energy. This result is comparable to energy barriers which have been determined for different solid-state phases of ferrocene, which vary from 5.4 to 24.8 kJ mol^{-1}.[59] The highest energy conformation is almost eclipsed, with the dihedral angle between methyl groups

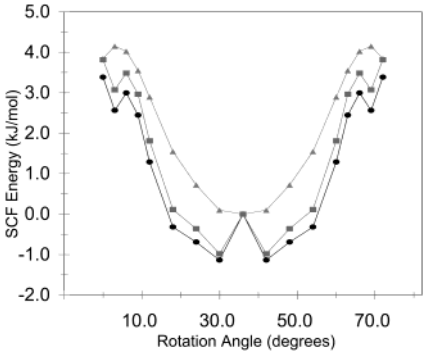

Figure 9. Rotational barrier: SCF energy versus relative dihedral angle between Cp* rings with D_{5h} being 0° from Gaussian 98 (▲) B3LYP/6-311G** geometry optimization, and (●) B3LYP/6-31G** and (■) B3LYP/6-311G** NMR calculations.

on opposing Cp* rings equal to 3°. The shape of the rotational barrier can be fit to the function $f(\theta) = A + B\cos(\theta - \pi/5)^2 + C\cos(\theta - \pi/5)^4 + D\cos(\theta - \pi/5)$,[6] where $A = 4.124(0.036)$, $B = -7.787(0.534)$, $C = 5.34(1.42)$, and $D = -1.714(0.969)$. The expectation value for the angle θ is $\langle\theta\rangle = 8.8576°$, meaning that the rings sit with methyl groups staggered at an angle of 27.14° with respect to one another. If the experimental rotational barrier is similar at room temperature in the solid state, the rings are undergoing restricted rotation, spending most of their time in a staggered conformation. Free rotation of the Cp* rings would require temperatures in excess of 498 K. The predominantly staggered conformation at room temperature is reflected by the measured anisotropic chemical shielding spans at room temperature.

To examine the origin of the chemical shielding interaction, it is useful to compare the diamagnetic and paramagnetic shielding contributions (see Table 4). Calculations on the staggered D_{5d} conformer of $[Cp^*_2Al]^+$ reveal that negative paramagnetic contributions responsible for deshielding the nucleus are much larger perpendicular to the five-fold molecular axis as compared with those along the molecular axis. Clearly, there must be occupied and virtual orbitals which are relatively closely spaced in energy that mix in the plane of the molecular axis to deshield the nucleus perpendicular to the molecular axis. Similar results are observed in the D_{5h} species, although the negative paramagnetic shielding contributions are reduced. Interestingly, comparison of calculations on both metallocene conformers with those on the hydrated Al^{3+} cation reveals that the latter has much larger negative paramagnetic shielding contributions, resulting in a deshielded aluminum nucleus (i.e., a high-frequency NMR shift).

(59) Kubo, A.; Ikeda, R.; Nakamura, D. *Chem. Lett.* **1981**, 1497.

Table 4. Theoretical Diamagnetic and Paramagnetic Contributions to Shielding at the Aluminum in $[Cp^*_2Al]^+$ and $Al(H_2O)_6^{3+}$

	σ_{11}^d	σ_{11}^p	σ_{22}^d	σ_{22}^p	σ_{33}^d	σ_{33}^p	σ_{iso}^d	σ_{iso}^p	σ_{iso}^{total}
$[Cp^*_2Al]^+$									
D_{5d} − staggered									
RHF/6-31G**	798.36	−76.80	798.36	−76.80	812.50	−19.61	803.08	−57.74	745.34
RHF/6-311G**	789.48	−70.15	789.48	−70.15	806.59	−16.82	795.19	−52.38	742.81
B3LYP/6-31G**	809.81	−126.84	809.81	−126.49	815.22	−50.75	811.62	−101.40	710.22
B3LYP/6-311G**	796.84	−124.68	796.84	−124.48	814.29	−55.25	802.66	−101.50	701.16
D_{5h} − eclipsed									
RHF/6-31G**	795.81	−55.51	795.81	−55.51	811.99	−26.03	801.21	−45.68	755.53
RHF/6-311G**	786.64	−49.68	786.64	−49.68	805.49	−19.71	792.92	−39.69	753.23
B3LYP/6-31G**	807.70	−103.60	807.70	−102.92	814.89	−62.51	810.10	−89.67	720.43
B3LYP/6-311G**	794.64	−102.10	794.64	−101.81	813.29	−62.93	800.85	−88.94	711.91
$Al(H_2O)_6^{3+}$									
RHF/6-31G**	785.57	−150.52	785.57	−150.52	785.57	−150.52	785.57	−150.52	635.05
RHF/6-311G**	781.79	−164.52	781.79	−164.52	781.79	−164.52	781.79	−164.52	617.27
B3LYP/6-31G**	789.71	−181.34	789.71	−181.34	789.71	−181.34	789.71	−181.34	608.37
B3LYP/6-311G**	787.40	−208.70	787.40	−208.70	787.40	−208.70	787.40	−208.70	578.70

Table 5. ADF Numerical Calculations of Contributions to Aluminum Chemical Shielding from Orbital Mixing

	$AlCl_4^-$	$Al(H_2O)_6^{3+}$	$[Cp^*_2Al]^+$
σ^{tot} (isotropic chemical shielding)	443.179	565.118	694.196
σ^d (total)	794.350	770.152	784.803
σ^d (core)	0.000	0.000	0.000
σ^d (valence)	794.350	770.152	784.803
σ^p (total)	−351.171	−205.034	−90.607
gauge invariance terms	−3.861	1.728	5.714
frozen core terms	0.000	0.000	0.000
σ^p (occ−occ)[a]	−70.642	2.589	132.316
σ^p (occ−vir)[a]	−276.668	−209.351	−228.637

[a] Occ−occ and occ−vir refer to contributions to paramagnetic shielding stemming from mixing of occupied MOs with occupied and virtual MOs, respectively.

To gain insight into which molecular orbitals in the aluminocenium cation are responsible for the aluminum chemical shielding anisotropy and high shielding of the aluminum nucleus, calculations were carried out with the ADF (Amsterdam density functional) software package (details are discussed in the Experimental Section of this paper). The results of the ADF BLYP calculations using basis set V are presented in Table 5 for three aluminum-containing species with markedly different isotropic chemical shifts, $AlCl_4^-$, $Al(H_2O)_6^{3+}$, and $[Cp^*_2Al]^+$. The isotropic chemical shielding values are in qualitative agreement with experimental data, with $[Cp^*_2Al]^+$ possessing the most magnetically shielded aluminum nucleus.

Under the GIAO formalism, diamagnetic and paramagnetic contributions are calculated independently from one another, with the former arising solely from ground-state electron circulation, and the latter arising from contributions from both the ground state and the magnetic-dipole-allowed mixing of ground- and excited-state wave functions. Commonly, the paramagnetic contribution arising from mixing of occupied and virtual molecular orbitals (occ−vir contribution) is the main factor causing variation in magnetic shielding among chemically distinct nuclei. However, ADF calculations indicate that a positive contribution (i.e., shielding) from the mixing of occupied wave functions (occ−occ) is of great significance for magnetic shielding at the aluminum nucleus in these complexes as well. The apparent origin of chemical shielding at the metal site in this p-block metallocene stands in stark contrast to that in a transition metal metallocene such as ferrocene.[55]

Before discussing $[Cp^*_2Al]^+$, we consider calculations of shielding tensors for two simple aluminum-containing species: $AlCl_4^-$ and $Al(H_2O)_6^{3+}$. Calculations on $AlCl_4^-$ indicate a large negative paramagnetic contribution to aluminum magnetic shielding from mixing of occupied MOs with other occupied MOs (occ−occ) and virtual MOs (occ−vir). The large occ−vir contribution stems from molecular orbitals heavily weighted with contributions from aluminum atomic orbitals. Specifically, occupied hybrid 2p-aluminum orbitals mix with virtual hybrid aluminum 2p and 3p orbitals, which are separated by approximately 10.3 eV. In the pseudooctahedral $Al(H_2O)_6^{3+}$ complex, the situation is similar, except that the occupied and virtual molecular orbitals which mix to give the largest negative paramagnetic contributions are separated by approximately 18.3 eV. Also, there is a small positive paramagnetic occ−occ contribution. In both cases, the high spherical symmetry of these complexes results in negligible magnetic shielding anisotropies.

The D_{5d} symmetry of $[Cp^*_2Al]^+$ lends itself to extremely different magnetic shielding environments perpendicular and parallel to the five-fold symmetry axis of the molecule. In this cation, the complicated p-π bonding at the aluminum center results in a cornucopia of positive and negative contributions to paramagnetic shielding from a variety of occ−occ and occ−vir symmetry-allowed mixing. For simplicity, we shall consider some of the larger contributions to the chemical shielding tensor (i.e., total contributions to the isotropic chemical shielding in excess of 18 ppm in absolute magnitude are given in parentheses; however, there are smaller contributions from occ−vir and occ−occ mixing of orbitals with similar symmetries). The larger contributions and the corresponding molecular orbitals are summarized in Tables 6 and 7, with three-dimensional contour images of the molecular orbitals pictured in Figure 10. Moderately large negative shielding contributions (ca. −19 ppm) perpendicular to the five-fold molecular axis come from mixing of two degenerate occupied $2E_{1u}$ MOs (comprised largely of contributions from $2p_{x,y}$ AOs on the aluminum atom) with the virtual $6A_{2u}$ and $8A_{2u}$ MOs, both of which have significant contributions from $3p_z$ aluminum AOs and smaller contributions from ring carbon p_z orbitals and hydrogen s orbitals. However, in comparison to $AlCl_4^-$ and $Al(H_2O)_6^{3+}$, the energy separations between occupied and virtual MOs are immense, with $E(2E_{1u} - 6A_{2u}) = 71.75$ eV and $E(2E_{1u} - 8A_{2u}) = 75.74$ eV. Furthermore, mixing of the occupied $2E_{1u}$

Table 6. Major Paramagnetic Shielding Contributions from Molecular Orbital Mixing

occ	vir	σ_{iso}	$\sigma_{\perp}$	$\sigma_{\parallel}$
$2E_{1u}$ (1)	$6A_{2u}$	−17.95	−53.9	0.0
$2E_{1u}$ (2)	$6A_{2u}$	−18.03	−54.1	0.0
$2E_{1u}$ (1)	$8A_{2u}$	−19.70	−59.1	0.0
$2E_{1u}$ (2)	$8A_{2u}$	−19.80	−59.4	0.0
$2E_{1u}$ (1)	$10A_{2u}$	30.32	90.9	0.0
$2E_{1u}$ (2)	$10A_{2u}$	30.44	91.3	0.0
occ	**occ**	σ_{iso}	$\sigma_{\perp}$	$\sigma_{\parallel}$
$2E_{1u}$ (1)	$2E_{1u}$ (2)	37.58	0.0	112.7
$2E_{1u}$ (1)	$3A_{2u}$	−39.98	−119.9	0.0
$2E_{1u}$ (2)	$3A_{2u}$	−40.14	−120.4	0.0
$5A_{2u}$	$5E_{1u}$ (1)	38.01	114.0	0.0
$5A_{2u}$	$5E_{1u}$ (2)	37.92	113.8	0.0
$5E_{1u}$ (1)	$5E_{1u}$ (2)	49.78	0.0	149.3

Table 7. List of Molecular Orbitals and Most Significant Symmetrized Fragment Orbitals

MO[a]	occ	energy (eV)	%[b]	SFO[c]	fragment
$2E_{1u}$ (1,2)	2	−74.50	99.98	$2p_{x,y}$	Al
$3A_{2u}$	2	−26.46	78.47	2s	C
			19.26	$2p_y$	C
			8.31	$3p_z$	Al
$5A_{2u}$	2	−14.11	83.50	$2p_z$	C
			6.82	$3p_z$	Al
$5E_{1u}$ (1,2)	2	−11.30	72.28	$2p_z$	C
			16.79	$3p_{x,y}$	Al
$6A_{2u}$	0	−2.74	57.30	$4p_z$	Al
			25.56	1s	H
			14.87	$3p_z$	Al
$8A_{2u}$	0	1.25	53.85	$4p_z$	Al
			28.40	$3p_z$	C
			20.66	$2p_z$	C
			18.77	$3p_z$	Al
$10A_{2u}$	0	5.74	36.44	$3p_z$	C
			20.54	2s	H
			20.25	$5p_z$	Al

[a] Molecular orbitals have symmetry labels corresponding to the D_{5d} point group. The "occ" column lists the electronic occupation of molecular orbitals (2 = occupied, 0 = virtual). [b] The % column denotes percent contribution to MOs from symmetry adapted atomic orbitals (AOs). [c] In the ADF software package, SFOs (symmetrized fragment orbitals) serve as the symmetry adapted basis set for the calculation (see ref 42c).

MOs with the virtual $10A_{2u}$ MO results in a positive paramagnetic shielding contribution perpendicular to the molecular axis (ca. +30 ppm). Along the molecular axis, there are no comparable large negative paramagnetic contributions, although there are a series of positive contributions arising from mixing of the occupied $2E_{1u}$ MOs with virtual MOs that possess substantial aluminum p-character.

Interestingly, occ−occ mixing of MOs with high $2p_z$ AO character from the Cp* ring carbons gives rise to both positive and negative paramagnetic shielding contributions. For instance, mixing of the degenerate $2E_{1u}$ MOs with the $3A_{2u}$ MOs produces large deshielding contributions (ca. −40 ppm, −120 ppm perpendicular to the molecular axis), while mixing of the degenerate $2E_{1u}$ MOs with one another shields the nucleus along the direction of the molecular axis (ca. +40 ppm, +120 ppm parallel to the molecular axis). Further, occ−occ mixing of the $5A_{2u}$ MOs (large contributions from Cp carbon $2p_z$ AOs and small contribution from the $2p_z$ Al orbital) with two degenerate $5E_{1u}$ MOs (Cp carbon $2p_z$ AOs and small contribution from the $3p_z$ Al orbital) provides heavy magnetic shielding of the aluminum nucleus (ca. +38 ppm, +114 ppm perpendicular to the molecular axis). Occ−occ mixing of the $5E_{1u}$ orbitals with one another shields the nucleus in the direction of the molecular axis as well (ca. +50 ppm, +149 ppm parallel to the molecular axis). Virtual rotation of ground- and excited-state orbitals is commonly used as a physical picture of magnetic-field-induced orbital mixing associated with a paramagnetic shielding contribution in a direction perpendicular to that rotation. However, there is no similar physical picture for mixing of occupied orbitals, although the shielding contributions occur in a direction perpendicular to their mixing. Nonetheless, occ−occ mixing of MOs localized on the Cp rings and not on the aluminum atom seems to play a major role in shielding the aluminum nucleus, as witnessed from the large positive paramagnetic contributions to the shielding tensor.

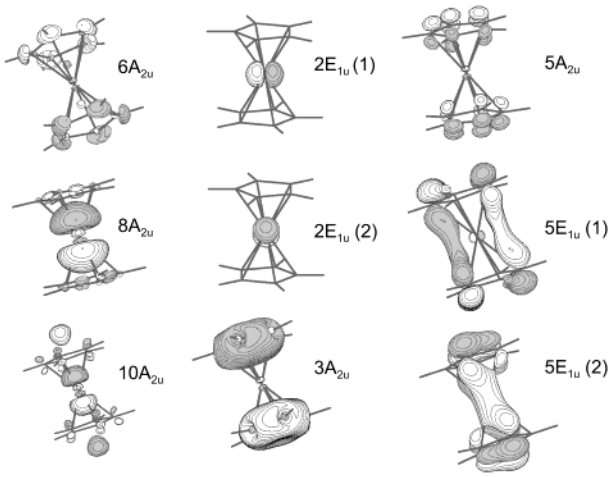

Figure 10. Occupied ($2E_{1u}$ (1,2), $3A_{2u}$, $5A_{2u}$, and $5E_{1u}$ (1,2)) and virtual ($6A_{2u}$, $8A_{2u}$, and $10A_{2u}$) molecular orbitals in $[Cp^*_2Al]^+$, which mix to make the largest aluminum paramagnetic shielding contributions. See text for full discussion.

Table 8. Experimental and Theoretical Carbon Shielding Tensors in $[Cp^*_2Al]^+$ [a]

	δ_{11} (ppm)	δ_{22} (ppm)	δ_{33} (ppm)	δ_{iso} (ppm)[b]	Ω (ppm)	κ
experimental	154.8(1)	154.8(1)	46.7(1)	118.7	108.1	1.00
theoretical						
RHF/6-31G**	174.77	127.54	22.49	108.27	152.28	0.38
RHF/6-311G**	173.63	123.68	11.93	103.08	161.69	0.38
B3LYP/6-31G**	182.47	141.30	44.28	122.68	138.19	0.40
B3LYP/6-311G**	182.35	141.27	44.22	122.61	138.13	0.41

[a] Absolute chemical shieldings are converted to chemical shifts with the formula $\sigma_{ref} - \sigma_{sample}$, where σ_{ref} is the absolute chemical shielding of CO. See Experimental Section for details. [b] $\delta_{iso} = (\delta_{11} + \delta_{22} + \delta_{33})/3$, $\Omega = \delta_{11} - \delta_{33}$, and $\kappa = 3(\delta_{22} - \delta_{iso})/\Omega$.

Theoretical Study of Carbon Shielding Tensors and Cp* Ring Dynamics in $[Cp^*_2Al]^+$. A comparison of experimental and theoretical carbon chemical shift tensors is presented in Table 8. With the exception of δ_{iso} and δ_{33}, comparison of the chemical shift tensor parameters reveals poor agreement between experimental and theoretical values. In all cases, the orientation of the chemical shift tensor at the Cp* ring carbons has the most shielded component, δ_{33}, perpendicular to the plane of the Cp* ring, and the least shielded component, δ_{11}, oriented along the direction of the methyl carbons. The discrepancy between experimental and theoretical values arises from the fact that the Cp* rings are undergoing rapid reorientation about the Cp* axis. It has previously been demonstrated that NMR powder patterns manifesting first- and second-order effects from aniso-

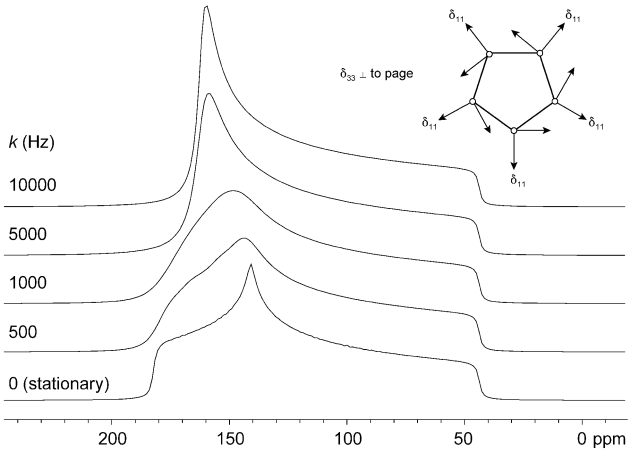

Figure 11. Simulations of ^{13}C static NMR powder patterns undergoing 5-fold chemical exchange. Inset: Picture of 5-fold ring and orientations of chemical shielding tensors determined from B3LYP/6-311G** calculations. See text for full discussion.

tropic chemical shielding tensors[60,61] and electric field gradient tensors[62,63] are influenced by both molecular motions and chemical exchange. Herein, a previously described semiclassical exchange formalism is used to treat the effects of chemical exchange on a powder pattern strongly influenced by first-order anisotropic chemical shielding.[61,63]

A static ^{13}C NMR powder pattern was simulated for the Cp* aromatic carbons using the chemical shift tensor values from the B3LYP/6-311G** calculation (Figure 11). Using the chemical shift tensor orientations described above, we found that the Euler angles for a five site exchange are $\alpha = 0, 2\pi/5, 4\pi/5, 6\pi/5, 8\pi/5$; $\beta = 0$ for all; $\gamma = 0$ for all. This corresponds to rotation of the orthogonal δ_{11} and δ_{22} components about a five-fold axis in 72° increments, leaving δ_{33} pointing along the axis of rotation, as illustrated in Figure 11. As the exchange rate is increased, the high-frequency portion of the powder pattern begins to collapse upon itself. At an exchange rate of $k = 5000$ Hz (one-half the breadth of the powder pattern), an axially symmetric pattern begins to take shape. Finally, at $k = 10\,000$ kHz, a powder pattern with a single sharp high-frequency discontinuity is present. The chemical shift tensor is analyzed to yield $\delta_{11} = \delta_{22} = 160(1)$ ppm and $\delta_{33} = 44(1)$ ppm, with $\delta_{iso} = 121.3$ ppm, $\Omega = 116$ ppm, and $\kappa = 1.0$, in very close agreement with experimental values.

Given the reliability of theoretical calculations of magnetic shielding tensors of first-row elements, and the remarkable correspondence between experimental and theoretical results, we believe that the combination of variable-temperature solid-state NMR, chemical exchange powder pattern simulations, and theoretical calculations of NMR interaction tensors may prove to be an excellent means of probing rotational barriers in a variety of organometallic complexes. Further variable-temperature ^{13}C and ^{27}Al NMR experiments are currently being conducted in our laboratory to study chemical exchange in this compound and other analogous systems.

Conclusion

A combination of solid-state ^{27}Al and ^{13}C NMR experiments and theoretical calculations of NMR interaction tensors has been used to study anisotropic NMR interaction tensors in the $[Cp^*_2Al]^+$ cation. The $[Cp^*_2Al]^+$ cation has a very small ^{27}Al quadrupolar interaction due to the high (D_{5d}) symmetry but a large aluminum chemical shielding anisotropy due to the cylindrical symmetry of this cation. Full analysis of the ^{27}Al satellite transition NMR spectra is required to measure the $C_Q(^{27}Al)$ because no second-order line shape was visible in the central transition MAS NMR spectra. Ab initio calculations of aluminum chemical shielding tensors are in excellent agreement with experimental values. Detailed RHF, B3LYP, and ADF BLYP calculations help to explain the large chemical shielding anisotropy and high magnetic shielding of the aluminum nucleus in $[Cp^*_2Al]^+$. In addition to negative paramagnetic shielding contributions from symmetry-allowed mixing of occupied and virtual orbitals, mixing of occupied MOs with other occupied MOs makes positive paramagnetic shielding contributions.

Calculation of carbon shielding tensors and chemical exchange simulations shows that rapid rotation of the Cp* rings results in an averaged chemical shielding tensor, which is observed experimentally. This methodology, and future variable temperature solid-state NMR studies on this system, may permit the precise measurement of the rotational barriers in a variety of metallocenes.

Acknowledgment. We thank Prof. Roderick Wasylishen (University of Alberta) for his helpful comments and the ARMRC (Atlantic Region Magnetic Resonance Centre, Dalhousie University) for NMR time on the 400 MHz spectrometer. We thank John D. Gorden and Silvia Filipponi (UT − Austin) for preparing some of the starting materials and salts. Prof. Doug Stephan (Windsor) is acknowledged for allowing us to use his gloveboxes for sample preparation. R.W.S. is grateful to Imperial Oil and the Natural Sciences and Engineering Research Council (NSERC Operations and Collaborative Research and Development grants) for funding this research project. R.W.S. also thanks the Canadian Foundation for Innovation, the Ontario Innovation Trust, and the University of Windsor for funding the new solid-state NMR facility at the University of Windsor. A.H.C. is grateful to the National Science Foundation (NSF) and the Robert A. Welch Foundation for financial support.

Supporting Information Available: Tables of X-ray crystallographic data and Cartesian coordinates used for ab initio calculations (PDF). This material is available free of charge via the Internet at http://pubs.acs.org.

JA020394P

(60) (a) Spiess, H. W.; Grosescu, R.; Haeberlen, U. *Chem. Phys.* **1974**, *6*, 226. (b) Spiess, H. W. *Chem. Phys.* **1974**, *6*, 217.
(61) Mehring, M. *Principles of High-Resolution NMR in Solids*; Springer-Verlag: Berlin, 1983.
(62) Witschas, M.; Eckert, H.; Freiheit, H.; Putnis, A.; Korus, G.; Jansen, M. *J. Phys. Chem. A* **2001**, *105*, 6808.
(63) Schurko, R. W.; Wi, S.; Frydman, L. *J. Phys. Chem. A* **2002**, *106*, 51.